Evidence for a Strong Surface-Plasmon Resonance on ErAs Nanoparticles in GaAs

E. R. Brown,[1] A. Bacher,[1] D. Driscoll,[2] M. Hanson,[2] C. Kadow,[2] and A. C. Gossard[2]
[1]*University of California Los Angeles, Los Angeles, California 90095-1594*
[2]*University of California Santa Barbara, Santa Barbara, California 91109*
(Received 1 May 2002; published 21 February 2003)

Room-temperature attenuation measurements are made between $\lambda = 0.8$ and 10.0 μm on three GaAs epitaxial samples containing layers of ErAs nanoparticles. An asymmetric attenuation peak is observed around 2.5 μm that increases in strength with ErAs density, and is modeled well by a Maxwell-Garnett formulation and semiclassical transport theory. The nanoparticles are assigned a distribution function of oblate spheroids having a minimum volume corresponding to a 1.0-nm sphere. This is consistent with the self-organizing tendency of ErAs in GaAs, and explains the sharp attenuation peak as a spherical-particle surface-plasmon (i.e., Fröhlich) resonance.

DOI: 10.1103/PhysRevLett.90.077403 PACS numbers: 78.30.Fs, 78.67.Bf, 78.67.De

Because of its high purity and direct band gap, GaAs remains one of the more useful materials to study the optical and optoelectronic effects of deep-level defects in bulk materials and surface states in nanostructures. One of the best means of forming bulk defects in GaAs has been low-temperature growth, LTG ($\sim 200\,^{\circ}$C), whereby excess As atoms are incorporated in the material during molecular-beam epitaxy (MBE) [1]. After annealing, many of the excess As atoms form precipitates, maintaining high crystallinity in the GaAs while creating very efficient nonradiative recombination centers and ultrafast photoconductivity. More recently, the useful optoelectronic characteristics of the LTG-GaAs have been obtained at normal growth temperature (535 °C) by incorporation of ErAs during the growth [2]. The ErAs self-organizes into nanometer-scale particles which act as fast recombination centers. The ErAs approach offers better control over the transport characteristics (e.g., the photocarrier lifetime) of the material.

We report here the measurements of the optical attenuation of the ErAs:GaAs material at photon energies well below the GaAs band edge. Three samples were measured at room temperature, each consisting of 30 layers of thin ErAs separated from each other by 40 nm of undoped GaAs. As listed in Table I, the samples differed only in the thickness of the ErAs layers of 0.8, 1.2, and 1.6 monolayer (ML) for samples 1, 2, and 3, respectively. All three were grown by MBE at 630 °C on semi-insulating (SI) GaAs substrates under conditions similar to those used in two previous studies. In the first study the ErAs deposition was varied over the same range as used here but the growth temperature was fixed at 535 °C [3]. This was the first study to show by microstructural techniques that ErAs layers form nm-sized nanoparticles about 3 to 4 ML (0.9 to 1.2 nm) high and about 1 to 2 nm in lateral dimension. The islands are isolated at low ErAs deposition (0.8 ML) and interconnected at high deposition (1.6 ML). In the second study the growth temperature was varied between 490 and 630° C, but the deposition was fixed at 1.8 ML—the highest deposition of the first study [4]. Again, the ErAs was found to form interconnected islands at 530 °C, but these became isolated in the sample grown at 630 °C. Transmission electron micrographs (TEMs) of the latter sample (which will be referred to below) proved that the islands are 3 to 4 ML (0.9 to 1.2 nm) thick and extend over a broad range up to $\sim$10 nm in the lateral dimensions. A small fraction of the particles extend over even a greater length in one in-plane direction, and are highly convoluted. The island density at 1.8 ML deposition is approximately 4×10^{11} cm^2. Because the present study involves three samples grown at 630 °C and having deposition of 1.6 ML or less, all three can be presumed to contain isolated nanoparticles. The changing deposition mainly affects the island density.

Optical transmission measurements were carried out with two instruments: a near-IR grating monochromator operating between $\lambda = 0.8$ and 2.5 μm, and a mid-IR Fourier-transform infrared (FTIR) spectrometer operating between 2.5 and 10 μm. Pieces of samples 1, 2, and 3

TABLE I. ErAs:GaAs material characteristics and assumed particle distribution parameters.

Sample	ErAs layer thickness (ML)	Fill fraction (%)	L_{min}	L_{max}	R	A	B
1	0.8	0.56	0.10	0.33	3.0	1.82	33.4
2	1.2	0.85	0.07	0.31	2.2	2.28	28.8
3	1.6	1.13	0.04	0.29	1.5	2.96	17.6

 0031-9007/03/90(7)/077403(4)$20.00

were mounted in metal holders and the transmission coefficient was determined by dividing the transmitted spectrum I_t by the incident spectrum I_i as measured by the instruments. To separate out attenuation effects in the epitaxial layer from the 500-μm-thick SI-GaAs substrate below it, the transmission through a bare double-side-polished SI-GaAs substrate from the same lot was also measured and used to normalize the spectra of the epitaxial samples. No fringes or strong attenuation were observed in the bare substrates for $\lambda > 0.9$ μm, so the primary effect of the normalization was to correct for the reflections from the two air-GaAs interfaces.

Plotted in Fig. 1 is the experimental normalized transmission measured through samples 1–3 between $\lambda = 0.8$ and 10 μm. To maximize data quality, the signal from 0.8 to 2.5 μm is taken from the grating spectrometer, and he signal from 2.5 to 10.0 μm is taken from the FTIR spectrometer. The dominant features in each spectrum are the precipitous GaAs band edge at ~0.85 μm and an asymmetric attenuation peak centered around 2.48, 2.55, and 2.59 μm for samples 1, 2, and 3, respectively. The attenuation strength grows between samples 1 and 3. The three curves also display spurious absorption bands centered around 2.6 and 6.5 μm that are attributed to residual H_2O vapor in the spectrometer, and a sharp feature at 4.3 μm attributed to CO_2.

Plotted in Fig. 2 is the attenuation coefficient derived from the normalized transmission. Since the epitaxial thickness is 1200 nm for each sample, the peak attenuation coefficient of the 2.5-μm attenuation feature is approximately 1300, 1850, and 2380 cm^{-1} for samples 1, 2, and 3, respectively. The asymmetry of this feature appears clearly as a long-λ tail having easily measured attenuation, even at $\lambda = 10$ μm. The peak attenuation values are surprisingly high considering that the material responsible for the attenuation, the ErAs layers, constitutes only about 1% of the epitaxial volume.

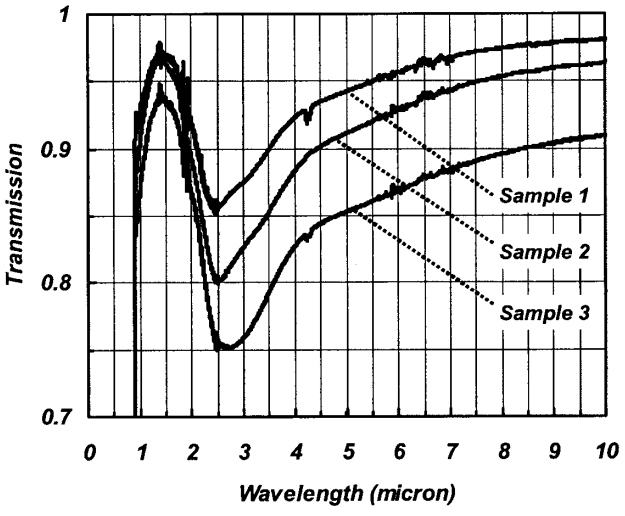

FIG. 1. Normalized transmission through three ErAs:GaAs samples at room temperature.

In constructing a theoretical model for the attenuation we have considered several possible mechanisms including free-carrier optical effects and quantum-size effects. The most accurate mechanism has been the free-carrier effects, which can be quite strong in small metallic or semimetallic particles when plasmon resonances occur [5]. Our free-carrier optical model treats the ErAs:GaAs epilayer as a composite medium consisting of independent ErAs nanoparticles separated by insulating GaAs. Consistent with previous experiments and theory [6], the ErAs is treated as a semimetal. The Drude model can be used to account for the free-carrier optics, so that the relative dielectric function of the ErAs is [7]

$$\varepsilon_S = \varepsilon_B - \frac{\omega_P^2}{\omega^2 + j\omega\gamma}, \tag{1}$$

where ε_B is the (real) background dielectric constant, ω is the circular optical frequency, ω_P is the plasma

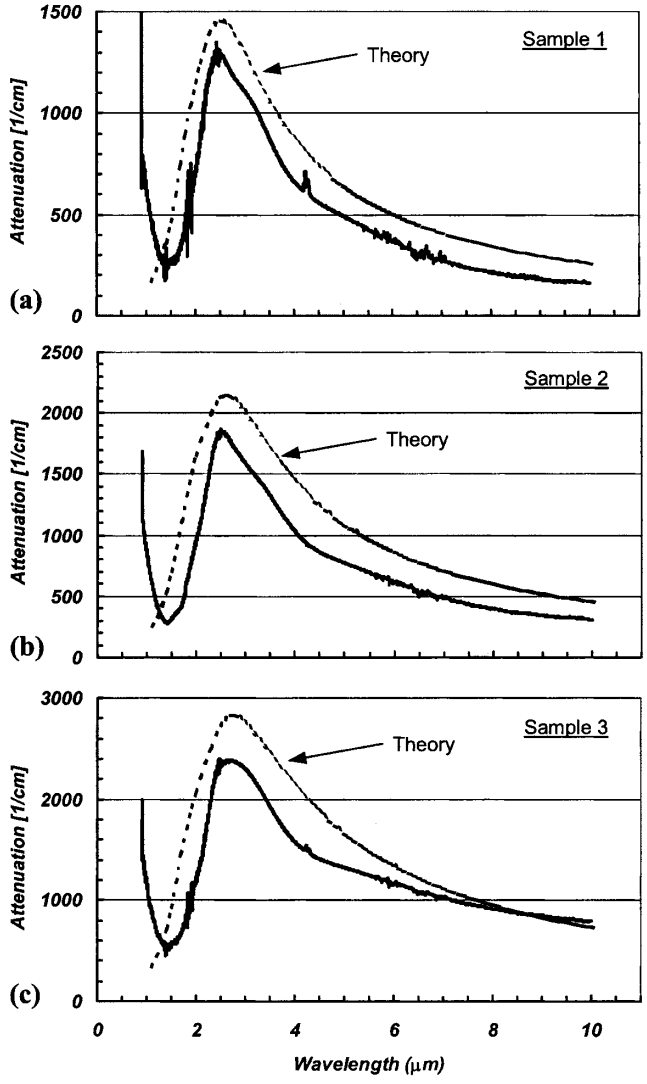

FIG. 2. Plots of experimental and modeled attenuation coefficient vs λ for the three ErAs:GaAs samples.

frequency, $\gamma\ (= 1/\tau)$ is the free-carrier scattering frequency, and τ is the scattering time.

In the composite medium the GaAs matrix is expected to modify the dielectric function in a manner that depends on the size and shape of the ErAs nanoparticles. In our case the ErAs particles are much smaller than λ. If we also assume that the ErAs particles occupy a relatively small fraction of the total material volume and are optically independent, we can apply the Maxwell-Garnett (MG) formulation. In its general form, the MG predicts a composite dielectric function of the form [5]

$$\varepsilon_{\mathrm{MG}} = \frac{(1-f)\varepsilon_M + f\beta\varepsilon_S}{1-f+f\beta}, \tag{2}$$

where f is the volumetric fill fraction of the ErAs component, and β is a numerical factor that depends on the size and shape of the ErAs nanoparticles. The intensity *absorption* constant then follows directly from the plane-wave solution to Maxwell's equations

$$\alpha = \frac{2\omega}{c}\,\mathrm{Im}\sqrt{\frac{\varepsilon_{\mathrm{MG}}}{\mu}}, \tag{3}$$

where μ is the complex magnetic permeability of the medium. Although ErAs is known to be paramagnetic at low frequencies, both it and the GaAs should display $\mathrm{Re}\{\mu\} \approx 1$ at the present infrared wavelengths.

Since our samples contain a broad distribution of nanoparticle sizes and shapes, the calculation of β is feasible only by a statistical analysis. We must infer a distribution function P in terms of independent variables that quantify particle sizes and shapes. If all particles are assumed to be ellipsoids, the independent variables are conveniently chosen as the geometric shape factors L_1, L_2, and L_3 along the three principal axes that satisfy $0 < L_1 < 1$. Then, one can write

$$\beta = \iint P(L_1, L_2)\,\frac{\xi_1+\xi_2+\xi_3}{3}\,dL_1 dL_2, \tag{4}$$

where $\xi_i \equiv \varepsilon_M/[\varepsilon_M + L_i(\varepsilon_S - \varepsilon_M)]$, P is normalized so that $\iint P(L_1, L_2)dL_1dL_2 = 1$, and the integration is not carried out over L_3 since it is constrained by the sum rule $L_1 + L_2 + L_3 = 1$ [5].

To estimate $P(L_1, L_2)$ we rely on the TEM micrograph taken on several ErAs:GaAs samples including the one similar to our sample 3 [2]. In all cases the nanoparticles are disklike with a thickness between 3 and 4 ML (0.85 to 1.1 nm) and a maximum lateral extent that depends on the ErAs deposition thickness and temperature, but is always much greater than the particle thickness. *An important and somewhat surprising aspect of the TEM imagery is the lack of very small particles.* The smallest observed lateral dimension of any particle is close, if not equal to, the particle thickness. And there is no preferred orientation of the disks within the plane of the ErAs. Thus we can approximate the nanoparticles as a distribution of *oblate* ellipsoids in which the eccentricity ranges between ≈ 1 and ≈ 0, corresponding to a range of L_1 and L_2 between ≈ 0 (very wide disk) and ≈ 0.33 (sphere). To account for variations of $P(L_1, L_2)$ within this range we adopt a functional form $P(L) = A + BL_i^2$, $L_{\min} < L_i < L_{\max}$, with A and B determined uniquely from two constraints: (i) $\iint P(L_1, L_2)dL_1dL_2 = 1$ and (ii) $P(L_{\max})/P(L_{\min}) = R$. The minimum spherical size of the nanoparticles may be caused by the self-organizing tendency of the ErAs growth under the MBE conditions of the present samples [8]. The self-organization is explicable by the immiscibility of ErAs and GaAs and the associated high energy thermodynamic state of many small particles compared to fewer large ones.

The fitting parameters $L_{\min}$, $L_{\max}$, and R are estimated by the following considerations. From the TEM micrograph corresponding to our sample 3, the disklike nanoparticles have a maximum lateral extent of approximately 20 nm, and a minimum lateral extent of approximately 2.0 nm. This leads to $L_{\min} = 0.04$ and $L_{\max} = 0.29$. Then from the higher occurrence of small particles over large ones, we set $R = 1.5$, leading to $A = 2.96$ and $B = 17.6$. Although TEM micrographs were not taken on samples 1 and 2, we can deduce qualitatively the effect on $P(L_1, L_2)$ from the difference in deposition. At half the deposition in sample 1 relative to sample 3, we expect a reduction in the maximum and minimum particle sizes of the distribution. If we assume that both go down by a factor of 2 and the thickness remains ≈ 1.0 nm, the minimum lateral dimension corresponds to $L_{\max} = 0.33$ (spherical) and the maximum dimension corresponds to $L_{\min} = 0.07$. Because of the expected preference for smaller particles in this sample, we assume $R = 3.0$ leading to $A = 1.82$ and $B = 33.4$. For sample 2 we simply assume distribution parameters intermediate to those of samples 1 and 3, as listed in Table I.

To estimate the absorption coefficient in our samples we compute Eq. (3) with input from (1), (2), and (4), and the nanoparticle parameters of Table I. The ErAs parameters ω_P, ε_B, and γ are not well known, so we determine them by a fitting procedure that starts with a theoretical or experimental estimate and then refines the estimate by requiring a match in peak attenuation λ, and a minimization of the deviation between the theoretical absorption spectrum and the experimental spectrum in Fig. 2. For example, a starting estimate of ω_P arises from a semiclassical analysis of crystalline ErAs in which the electrons in the conduction band and holes in three valence bands (light hole, heavy hole, and split-off) all contribute to the transport. Fortunately, the carrier concentrations and effective masses are known: $\rho\ [\mathrm{cm}^{-3}]$, $m^*/m_e = 4.14 \times 10^{20}$, 0.21; 1.19×10^{20}, 0.28; 2.93×10^{20}, 0.46; and 0.02×10^{20}, 0.15 for the electrons, light holes, heavy holes, and split-off holes, respectively [6]. From these ω_P is found to be 3.1×10^{15} Hz, corresponding to a λ of 0.61 μm. This is considerably longer than the plasma cut-off in most metals since the total carrier

TABLE II. GaAs and ErAs fitting parameters.

Parameter	Starting value	Final value
ε_M	10.9	10.9
ε_B	22	25
ω_P [s^{-1}]	3.1×10^{15}	5.6×10^{15}
λ_P [μm]	0.61	0.34
γ [s^{-1}]	3.0×10^{14}	4.0×10^{14}
τ [fs]	3.3	2.5

concentration in the ErAs (8.3×10^{20} cm^{-3}) is so much lower (e.g., in copper $\rho = 8.4 \times 10^{22}$ cm^{-3}).

The starting value of the background dielectric constant ε_B of ErAs is chosen in comparison to the high-frequency limit ε_∞ of two similar materials—InAs and PbTe. InAs is an atomically similar material having $\varepsilon_\infty \approx 12.3$. PbTe is a structurally similar (rocksalt) material having $\varepsilon_\infty \approx 32$ [9]. So in the fitting procedure we start with an intermediate value $\varepsilon_B = 22$. Finally, for λ we start with a value that accounts for both bulk and surface effects. A useful approximation is $\gamma = \gamma_{\text{bulk}} + \gamma_{\text{surf}} \approx \gamma_{\text{bulk}} + \langle v_F \rangle / d$ where $\langle v_F \rangle$ is the Fermi velocity averaged over carrier types and d is the dimension between the opposing surfaces that cause the most scattering. γ_{bulk} can be estimated from measurements on the conductivity of ErAs films on GaAs at room temperature, $\sigma \approx 1.5 \times 10^4\ \Omega^{-1}\ \text{cm}^{-1}$ [10], and the Drude model, which yield $\gamma_{\text{bulk}} = 1.05 \times 10^{14}\ \text{s}^{-1}$ or $\tau_{\text{bulk}} = 9.9$ fs. A maximum estimate of the surface scattering results by setting d equal to the minimum dimension of the nanoparticles—the thickness. Like the plasma frequency, v_F of ErAs is found by averaging the v_F of individual carriers over all four bands, leading to $\langle v_F \rangle = 1.14 \times 10^6$ m/s. For nanoparticles all having a thickness of ≈ 1 nm, we find a maximum of $\gamma_{\text{surf}} \approx 1.1 \times 10^{15}$ ($\tau = 8.8 \times 10^{-16}$ s), well above the bulk value. So for the fitting procedure we start with an intermediate value $\gamma = 3 \times 10^{14}$ ($\tau = 3.3 \times 10^{-15}$ s).

Table II lists the final values of the ErAs parameters obtained by the fitting procedure. Figure 2 shows the theoretical fitted curves of attenuation coefficient in comparison to experiment for each of the three samples. The best agreement occurs for sample 1. The theory displays the precipitous rise of attenuation between 1.5 and 2 μm, the pronounced peak at 2.5 μm, and the long-λ tail extending to 10 μm and beyond. The peak theoretical attenuation is greater than experiment by 12%. The comparison for sample 2 is similarly good in the spectral shape, with an attenuation peak occurring at 2.6 μm. But the theoretical peak is now 18% greater than experiment. The comparison for sample 3 shows good agreement for the precipitous rise and peak attenuation at 2.7 μm, with the theoretical peak still only 18% above the experiment. But the long-λ tail now falls significantly faster than the experiment. In comparing the experimental curves of Figs. 2(b) and 2(c), it is apparent that sample 3 displays a more gradual long-λ tail than sample 2. One possible explanation for this is the small fraction of long convoluted particles that exists in this sample. Another explanation may be in-plane electromagnetic coupling between the nanoparticles that would violate the isolation requirement of the Maxwell-Garnett formalism. Although the volumetric density of ErAs in sample 3 is just over 1%, the in-plane density within the 3 to 4 nm ErAs nanoparticle layer thickness is much higher—roughly 40 to 50%.

In conclusion, we further elucidate the nano-optics behind the proposed effect. It is well known that metallic particles dispersed at low fill fraction in an insulating host can display resonant attenuation below the bulk plasma frequency associated with electromagnetic modes of the particle. When the modes are quantized, they become the so-called surface plasmons. Remarkably, the fundamental mode of our smallest (spherical) nanoparticles can be predicted directly from the MG theory. In this case it is straightforward to show that $\beta = 3\varepsilon_M/(\varepsilon_S + 2\varepsilon_M)$, and then (2) displays a pole in the dielectric function at the frequency where $\varepsilon_S \approx -2\varepsilon_M$ [11]. According to (1), when $\gamma \ll \omega$ the frequency that satisfies $\varepsilon_S \approx -2\varepsilon_M$ is simply $\omega = \omega_p/(\varepsilon_B + 2\varepsilon_M)^{1/2} \equiv \omega_F$, often called the Fröhlich resonant frequency [12]. In the present samples with a fitted value $\omega_p = 5.6 \times 10^{15}$ Hz, $\lambda_p = 0.34$ μm, $\varepsilon_M = 10.9$, and $\varepsilon_B \approx 25$, we find $\omega_F = 8.2 \times 10^{14}$ Hz and $\lambda_F = 2.3$ μm, in good agreement with the peak of the model attenuation curves. And note that our estimation for γ of $4 \times 10^{14}\ \text{s}^{-1}$ is over 2 times smaller than ω_F, so we expect the coherence requirement on quantization, $\omega_F \tau \gg 1$, to be satisfied even at room temperature.

[1] F.W. Smith, A. R. Calawa, C. L. Chen, M. J. Manfra, and L. J. Mahoney, IEEE Electron Device Lett. **9**, 77 (1988).
[2] C. Kadow *et al.*, Appl. Phys. Lett. **75**, 3548–3550 (1999).
[3] C. Kadow *et al.*, J. Vac. Sci. Technol. B **18**, 2197 (2000).
[4] C. Kadow *et al.*, J. Vac. Sci. Technol. B (to be published).
[5] C. F. Bohren and D. R. Huffman, *Absorption and Scattering of Light by Small Particles* (Wiley, New York, 1983).
[6] W. R. L. Lambrecht, B. Segall, A. G. Petukhov, R. Bogaerts, and F. Herlach, Phys. Rev. B **55**, 9239 (1997).
[7] N.W. Ashcroft and N. D. Mermin, *Solid State Physics* (Holt, Rinehart, and Winston, New York, 1976).
[8] K. E. Singer, P. Rutter, A. R. Parker, and A. C. Wright, Appl. Phys. Lett. **64**, 707 (1994).
[9] C. Kittel, *Introduction to Solid State Physics* (Wiley, New York, 1976), 5th ed., pp. 308–309.
[10] J. Ralston *et al.*, J. Electron. Mater. **19**, 555 (1990).
[11] H. Fröhlich, *Theory of Dielectrics* (Oxford University Press, London, 1949).
[12] Note: when $\varepsilon_B = \varepsilon_M = 1$, ω_F reduces to $\omega_p/(3)^{1/2}$, the resonance frequency for a sphere in vacuum.